

THE LOW FREQUENCY VIBRATION OF A RIBBED CYLINDER, PART 2: OBSERVATIONS AND INTERPRETATION

C. H. HODGES, J. POWER AND J. WOODHOUSE

Topexpress Limited 13/14 Round Church Street, Cambridge CB5 8AD, England

(Received 24 May 1984, and in revised form 10 September 1984)

The vibratory behaviour of ribbed cylinders is discussed. Very good agreement has been obtained between theoretical modelling described elsewhere [1] and measurements on a ribbed cylinder over a frequency range from zero to about three times the ring frequency. The first three pass bands for vibration transmission along the cylinder occur in this frequency range, associated with the first two resonant modes of a single bay of the structure and with a cross-sectional resonance of the T-section ribs. The position and nature of these three bands as a function of circumferential wavenumber are studied. Also the group velocity as a function of frequency and wavenumber is studied, and agrees in considerable detail with that obtained from measured sonograms.

1. INTRODUCTION

This paper summarizes an extensive series of measurements of the vibration of a ribbed cylinder carried out in order to validate theoretical modelling described in an accompanying article [1]. A uniform cylinder divided into 44 nominally identical bays by T-section ribs, and closed by partial-sphere caps at both ends, was used in the measurements. A sketch of the geometry is given in Figure 1 of reference [1]. The vibrational behaviour of this cylinder has been studied in the frequency range from zero up to about three times the ring frequency.

The behaviour revealed is quite complicated. Since it is desired to make very detailed comparisons between theory and measurements, it is necessary to have a firm grasp of the qualitative features of this behaviour. Consequently, the next section is devoted to developing such a qualitative description of ribbed cylinder behaviour. Then the experiments are described in section 3, and some of the results are presented and the comparison with theory discussed in section 4. The complete set of measurements is far too voluminous to reproduce here, but sufficient examples of the results are shown in this article for a convincing validation of the theoretical modelling.

As a result of the interplay of theory and measurement, it was found necessary to take into account a range of details of the geometry of the ribbed cylinder which at first sight one might have expected not to matter at these relatively low frequencies. In particular, important physical effects were observed which necessitated allowing for internal degrees of freedom of the T-section ribs.

By far the clearest experimental pictures of how the ribbed cylinder behaves come from sonograms. These also provide the most stringent and detailed check of the theoretical modelling. The application of sonograms to structural acoustics is slightly out of the ordinary, and the use to which they can be put in this kind of problem has recently been described in another article [2].

2. AN OUTLINE OF RIBBED CYLINDER BEHAVIOUR

An unribbed cylinder has a series of different modes of wave propagation, each associated with a different circumferential variation. In terms of cylindrical polar coordinates (r, θ, z) and time t , the components of displacement have the dependence $\cos n_c \theta \cos(kz - \omega t)$ where ω is frequency and k is axial wavenumber. The variable n_c obviously has to be an integer, and the values $0, 1, 2, \dots$ give the succession of waveguide modes. The theory of the low frequency vibration of unribbed cylinders has been described by Arnold and Warburton [3].

Recently measurements have been presented similar to those which are about to be described, carried out on an unribbed cylinder, and have been compared with that theory [2] in the article describing the sonogram technique referred to above. The comparison was very satisfactory. A brief account is also given there of the behaviour of unribbed cylinders, which need not be reiterated here. The only feature one needs to note is that, as with other waveguide problems, for values of n_c of 2 or greater there is a cut-off frequency below which waves with that circumferential dependence cannot propagate: this cut-off is the resonant frequency of a bending ring with the appropriate value of n_c given [4] by

$$\omega_0 \propto n_c(n_c^2 - 1)(n_c^2 + 1)^{-1/2}. \quad (1)$$

For all frequencies above this, waves can propagate along the cylinder in that waveguide mode.

2.1. THE EFFECT OF SIMPLY-MODELLED RIBS

The addition of regularly spaced ribs to the cylinder preserves the cylindrical symmetry of the problem, so that separability of z and θ dependence still applies; one continues to characterize the different propagation modes by their respective values of n_c . For a given n_c , however, the response of the ribbed cylinder as a function of frequency differs significantly from that of the unribbed cylinder; whereas before one had propagation at all frequencies above the cut-off, one now finds a sequence of stop bands appearing which break up the frequency range for transmission into a series of discrete pass bands [5]. The behaviour within a given pass band is governed by Bloch's theorem, as discussed in the Introduction of reference [1]. The bay-to-bay variation of displacement is controlled by the Bloch (or Floquet) wavenumber.

Broadly speaking, for a given mode of propagation along the cylinder one gets a stop band every time the axial length-scale of the response fits the rib spacing. Thus there is one near the frequency where a half-wavelength along the cylinder fits between two ribs, then again when two half-wavelengths fit, and so on. The behaviour to be expected for simply-modelled ribs (i.e., with their internal degrees of freedom neglected) is summarized schematically in Figure 1. What is plotted here is the n_c - ω plane, showing frequencies for which propagation can occur at different values of n_c . For a particular value of n_c there is a sequence of pass bands and stop bands indicated by the shaded and unshaded regions respectively. Actually, of course, discrete vertical lines should have been drawn for the separate n_c values since n_c is not a continuous variable, but for clarity continuous lines are shown for the band edges and the regions of pass bands are shaded. This picture does not represent any particular model in detail, but it shows the qualitative effect of periodic constraint by the ribs.

Figures 2(a)-(l) show sketches of the displacement shapes of the ribbed cylinder in the axial direction on the various band edges at the points labelled (a)-(l) in Figure 1. One can gain a number of useful qualitative insights from these two figures, which will

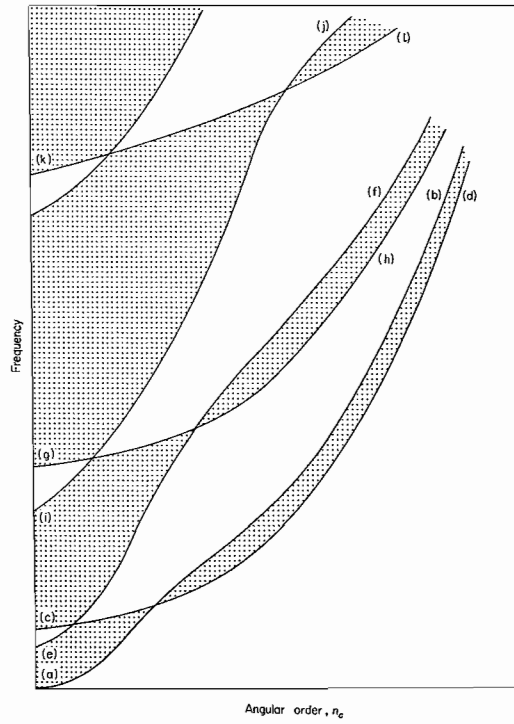


Figure 1. Sketch of the expected positions of pass bands (shaded) on a ribbed cylinder as a function of n_c . The letters in brackets refer to Figure 2.

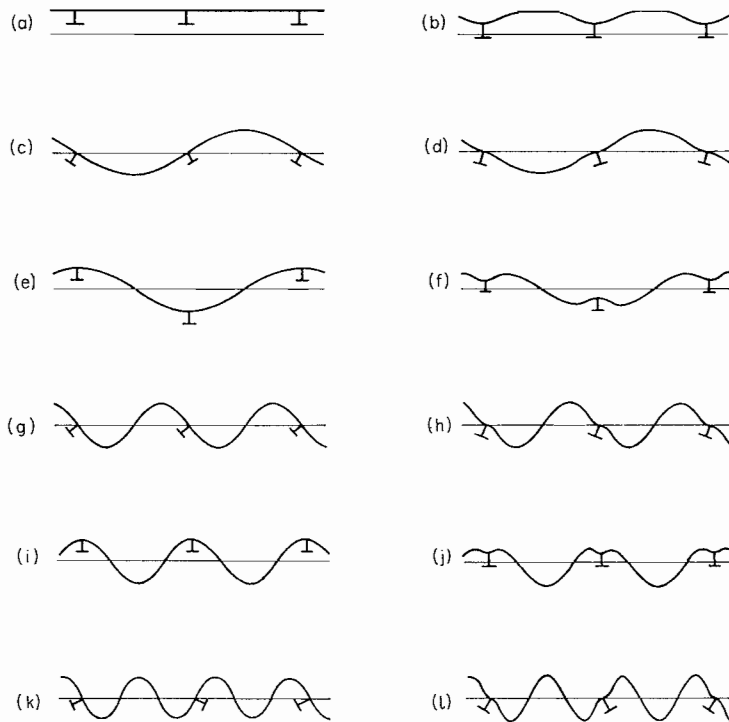


Figure 2. Sketch of the motion of the ribbed cylinder at the points labelled (a)-(l) in Figure 1.

help later when one looks at the more complicated picture corresponding to Figure 1 for the actual model. They will also be vital in interpreting the different measurements made on the ribbed cylinder to test the theory.

The reason for drawing the configuration of the cylinder at both ends of each line in Figure 1 is that there is a significant change of character between these two ends: this is evident in the transition from rather narrow stop bands at the left-hand side of the figure to narrow pass bands at the right-hand side. Comparing Figures 2(a) with (b), (c) with (d) and so on, one sees that as one moves along any line in Figure 1 from left to right the ribs move less (because their resistance to bending and twisting increases with n_c) so that the motion of the cylinder becomes relatively greater. It is convenient to classify lines in Figure 1 according to whether the motion at the ribs is predominantly *bending* (in the direction at right angles to the page in Figure 2) or *twisting*. Thus (a)-(b) and (e)-(f) are bending lines, while (c)-(d) and (g)-(h) are twisting lines. These two classes of lines behave differently as functions of n_c . (This bending-twisting distinction is related to a more general classification of types of coupling in periodic systems made by Mead [6].)

The picture is easiest to understand at the right-hand side. Here the ribs move very little, so that the adjacent bays on the cylinder are only weakly coupled together. This produces a series of narrow pass bands, one based on each mode of an individual bay when clamped at the ribs, very similar to the sequence of bands on a periodically mass-loaded string discussed in some detail for example in reference [7], section 2 and Figure 2(a). The two edges of each band are marked by equal amplitude in all bays, one edge having motions of the same sign in each bay and the other edge alternating sign in successive bays (in other words, zero Bloch wavenumber and Nyquist Bloch wavenumber). For this regime on the right-hand side of the figure, one can use an argument similar to that at the end of section 2 of reference [7] to see that the edges at which the ribs bend ((b), (f), etc.) lie at a higher frequency than the edges at which the ribs twist ((d), (h), etc.), as shown. This is because the constraining action of the ribs is stronger in bending than twisting, and thus keeps the frequency closer to the clamped-clamped frequency.

As one moves across the picture towards the left-hand side, the constraining effect of the ribs decreases and the behaviour becomes more like that of an unribbed cylinder. Motions (d), (h) and (l), all involving twisting at the ribs, do not change very much with decreasing n_c . The only significant changes in the motion are near the ribs, due to a loss of near field components associated with the clamping action of the ribs. This leads to a reduction of wavenumber on the plate and thus to a drop in frequency of the motions labelled (c), (g) and (k).

Motions such as (b), (f) and (j), involving bending of the ribs, are affected much more strongly by decreasing n_c . Relaxing the rib constraint eliminates one half-wavelength of the cylinder displacement in each bay as well as nearfield components. Thus the curves starting at (f), (j) and so on approach respectively those starting at (d), (h), etc., one clamped bay resonance down, as n_c becomes small.

In fact, those curves in the range plotted cross for sufficiently small n_c . One can make this plausible by considering $n_c = 1$. Any radial motion of the ribs with this particular n_c consists simply of a rigid body displacement, and thus involves no potential energy of the ribs. Comparing the motions (c) and (e), one sees that they both involve the same motion of the cylinder (and therefore the same associated potential and kinetic energies of the cylindrical shell), but (c) has potential energy of twisting of the rib while (e) has no potential energy of bending of the rib. Thus, provided the kinetic energy of rib twisting is not much greater than the that due to rib displacement the ratio of total potential to kinetic energy is reduced, and so (e) must be at a lower frequency than (c) as shown in Figure 1.

2.2. INTERNAL DEGREES OF FREEDOM OF THE RIBS

One now has a qualitative understanding of the behaviour of the ribbed cylinder when one models the ribs simply with passive added stiffness and mass for bending and twisting motion. However, the shape of the T-section ribs allows more complicated behaviour in which the cross-section of the ribs exhibits resonant modes. The lowest of these cross-sectional resonances, in which the web of the rib bends as a cantilever, lies within the frequency range under study for the particular geometry of the experimental ribbed cylinder. Its effect is to modify Figure 1 into something similar to Figure 3.

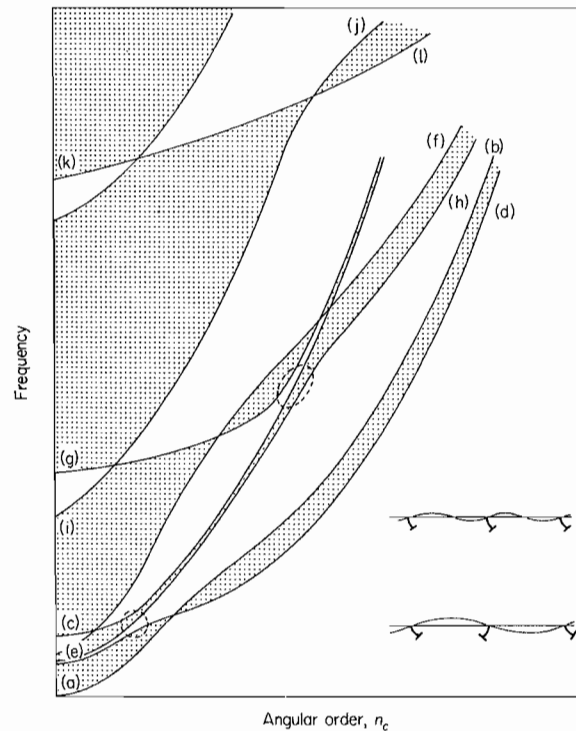


Figure 3. As Figure 1, but including the rib resonance band and its coupling with other lines in the figure (coupling occurs in the regions indicated by dashed rings). Also shown are sketches of the cylinder motion at the edges of the rib resonance band, on top at zero wavenumber, on the bottom at the Nyquist wavenumber. Band edges are labelled with letters as in Figure 1.

One can understand this picture as the coupling of a narrow pass band associated with the rib resonance with the pass bands already discussed. The band is narrow because the coupling of adjacent ribs through the intervening cylinder is quite weak. For all values of n_c the rib resonance implies bending motion of the rib flange, and as n_c increases the band moves up in frequency due to the increasing bending energy. In the bottom right-hand corner of Figure 3 are sketches showing roughly the motion of the ribs and cylinder along the two edges of this band.

The form of the coupling between the two types of bands can be deduced from the sketches of motion at the band edges. First one can note that displacements with different symmetries (symmetric and antisymmetric about the ribs) do not couple, so that symmetric motions in Figure 2 described previously as rib bending (rather than rib twisting) remain unchanged. One can next look in Figure 3 for places where two lines having the same

symmetries in their motion sketches would cross in the absence of any coupling. The effect of coupling between modes which are nearly degenerate is to split the eigenvalues and to produce repulsion between the lines in the region of the crossing. Each edge of the rib resonance band couples to just one line in Figure 1. The edge of the rib resonance band involving the same sign of motion in each bay corresponds to line (g)-(h) in Figure 1, and the edge involving opposite signs from bay to bay corresponds to line (c)-(d). In order to make the process clear, the pairs of lines which have coupled together and repelled are indicated in Figure 3 by dashed rings. These lines now join up differently—mode mixing allows the rib resonance to change continuously into rib twisting and vice versa. A curious point to note is that in this picture what have been thought of as the edges of the rib resonance band do not always form the top and bottom edges of a pass band—sometimes they delineate a stop band!

The rather complicated resulting picture, which one can now understand in qualitative detail, will provide guidance in interpreting the detailed theory and measurements to be given in section 4. One should note that Figure 3 shows a larger range of frequency and n_c than will be followed in detail: the measurements and the numerical calculations cover rather less than half the frequency range shown in Figure 3, and about half the range of n_c . This is enough to encompass the first three bands, the first two clamped bay resonances and the rib resonance, and thus to give a thorough test of understanding.

3. THE MEASUREMENTS

In this section the measurements taken on the ribbed cylinder to test the theoretical work are described. To provide a direct comparison with the theory, one first needed to separate the vibrational behaviour of the cylinder corresponding to the different values of n_c . The method of doing this was the same as described previously for measurements on an unribbed cylinder [2]: to measure response to an impulsive source on an array of sensors spaced uniformly around the circumference of the cylinder, and Fourier analyze the results with respect to azimuthal angle θ . This process is called here "angular filtering".

For practical convenience the measurements were made reciprocally, by using one accelerometer at a fixed position and tapping at points around the circumference by using a force transducer hammer. Measurements were made at 32 points, a convenient power of two for FFT purposes, giving a spatial Nyquist limit at $n_c = 16$. Most of the measurements were made with a soft-tipped hammer, so that the energy input was concentrated in the frequency range covered by the theory. All spectra and sonograms to be presented have the same frequency scale, linear from zero to three times the ring frequency.

From the sketches of mode-shape configurations in Figure 2 it is apparent that in order to see all possible motions of the ribbed cylinder, one needs to make measurements in more than one position since for any given position certain types of motion will be weak there, and therefore not easily seen in the measurement. The three places shown in Figure 4 were chosen: radial in the centre of a bay, radial on a rib and axial on the flange of a rib. Thus a series of measurements has been obtained for radial tapping at 32 positions around the centre of a bay, observed by an accelerometer mounted radially in the centre

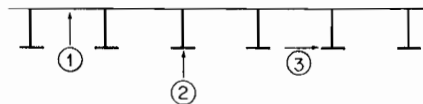


Figure 4. The three positions used for exciting and observing the ribbed cylinder: number 1 is the bay centre, number 2 is normal on the rib, and number 3 is on the side of the rib.

of another bay, and two similar series for the other positions. For each series, measurements were made over three different lengths of the cylinder—typically bay 6 to bay 37, bay 6 to bay 20 and bay 6 to bay 6 (driving bay measurements). (To avoid complications, the measurement points were kept a few bays away from both ends of the cylinder.)

Thus nine sets of measurements were produced, each set consisting of 17 angular filtered time series for the values of n_c from zero to 16. These time series have been analyzed in two different ways. First, ordinary power spectra were calculated from each time series. Second, for the measurements not in the driving bay, sonograms were plotted over a rather short time range to show the first arrival time as a function of frequency for each value of n_c . It turns out that the sonograms give much clearer pictures of what is going on in the cylinder following an impulse, and a much more convincing test of the theory than the power spectra. However, the latter are still useful, since with their greater frequency resolution they enable edges of pass bands to be located with greater precision.

An introduction to the use of sonograms in the analysis of structural vibration has been given elsewhere [2]. The main virtue of the method is that it gives a direct measure of group velocity as a function of frequency. For a single pass band, the shape one expects to see in the sonogram is a "horse-shoe". The reason is that the modes cluster at the edges of the band so that the group velocity goes to zero there, and rises to a maximum somewhere around the band centre. The precise shape of the horse-shoe depends on what happens to the modal distribution, and it will be seen in the measurements that bands can vary from very simple, symmetric shapes to rather complicated ones with more than one maximum of group velocity in the band.

It was stated above that sonograms give clearer pictures than power spectra. One important reason for this concerns departures of the geometry of the ribbed cylinder from ideal cylindrical symmetry. This non-ideality introduces some weak coupling between the different values of n_c . As a result there is scattering between the different angular orders and, although the coupling is weak, this scattering can build up progressively over a long time interval. For a power spectrum one uses a much longer section of the time series than for a sonogram in order to achieve better frequency resolution, and thus it is much more contaminated than the sonogram by the energy which has scattered progressively from other angular modes.

4. COMPARISON OF MEASUREMENTS AND THEORY

For each value of n_c from zero to 16, the raw data was processed to produce a set of measured spectra and sonograms for the three driving positions measured in bay 20, and the driving-bay spectrum in bay 6 for excitation on the side of the rib. These spectra and sonograms have been used to deduce band edge positions to compare with the theoretical predictions of reference [1].

4.1. BAND EDGE DATA

The comparison of measured and predicted pass band positions is shown in Figure 5. The experimental results are shown as lines joining crosses. The theoretical predictions are shown in a different form to the version given in Figure 3 of reference [1], in an attempt to make the comparison clear. Vertical lines of symbols are plotted, corresponding to every other mode of the structure. These collectively correspond to the shaded regions in Figure 3. It can be seen quite clearly that the extent of overall agreement between theory and experiment is very good.

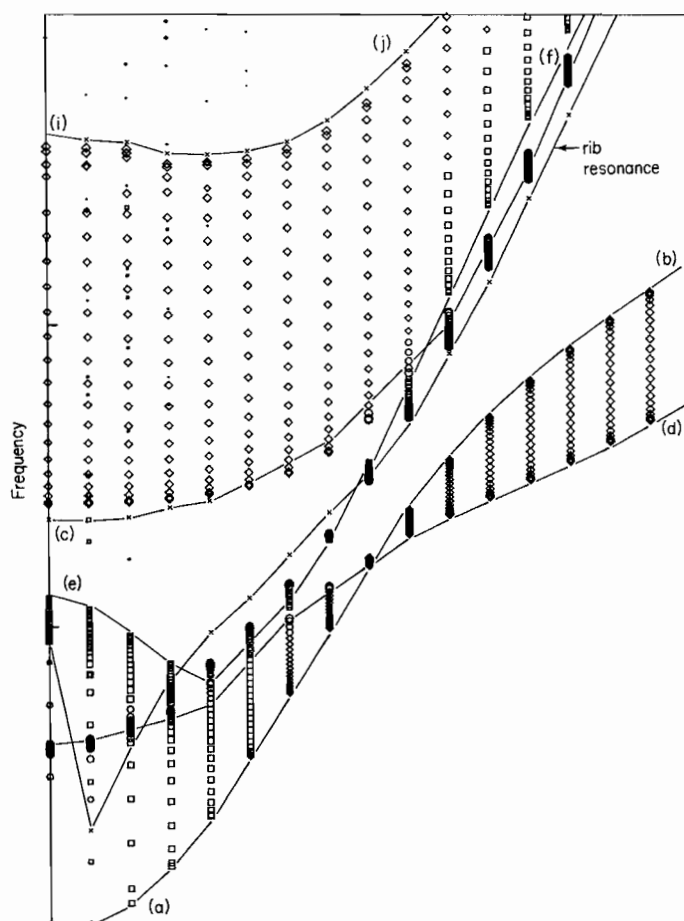


Figure 5. Comparison of theoretical pass band positions (lines of plotted symbols) with measured ones (crosses joined by lines). Band edges are labelled to correspond to Figures 1-3. Ticks on the frequency axis show multiples of the ring frequency.

It is easy to relate the features in Figure 5 to corresponding ones in the qualitative version, Figure 3. To facilitate comparison of these two figures, the labelling (a), (b), etc., has been indicated on Figure 5. However, there are two differences which are worth commenting on. First, in building up the qualitative picture of ribbed cylinder behaviour no discussion was given of the in-surface compressive and shear motion of the cylinder shell. Modes predominantly of this character are sparse in frequency and have little influence on the measurements, which are concerned only with radial motion of the shell. These in-surface modes are included in the full theory [1], but their effect has been largely suppressed in Figure 5 by varying the sizes of the plotted symbols so that such modes appear only as small dots.

The second difference is the initial dip in frequency of line (e)-(f) as n_c increases from zero. This is a result of the asymmetric placement of the rib on one side only of the cylindrical shell, and is discussed in detail in reference [1], section 5. Essentially, the resistance of the shell to in-surface shear constrains its motion to be radial at the Nyquist wavenumber. At $n_c \approx 4$, where the mode frequency is a minimum, radial motion of the shell is compatible with a neutral axis for rib bending lying in the flange, thus eliminating most of the bending energy.

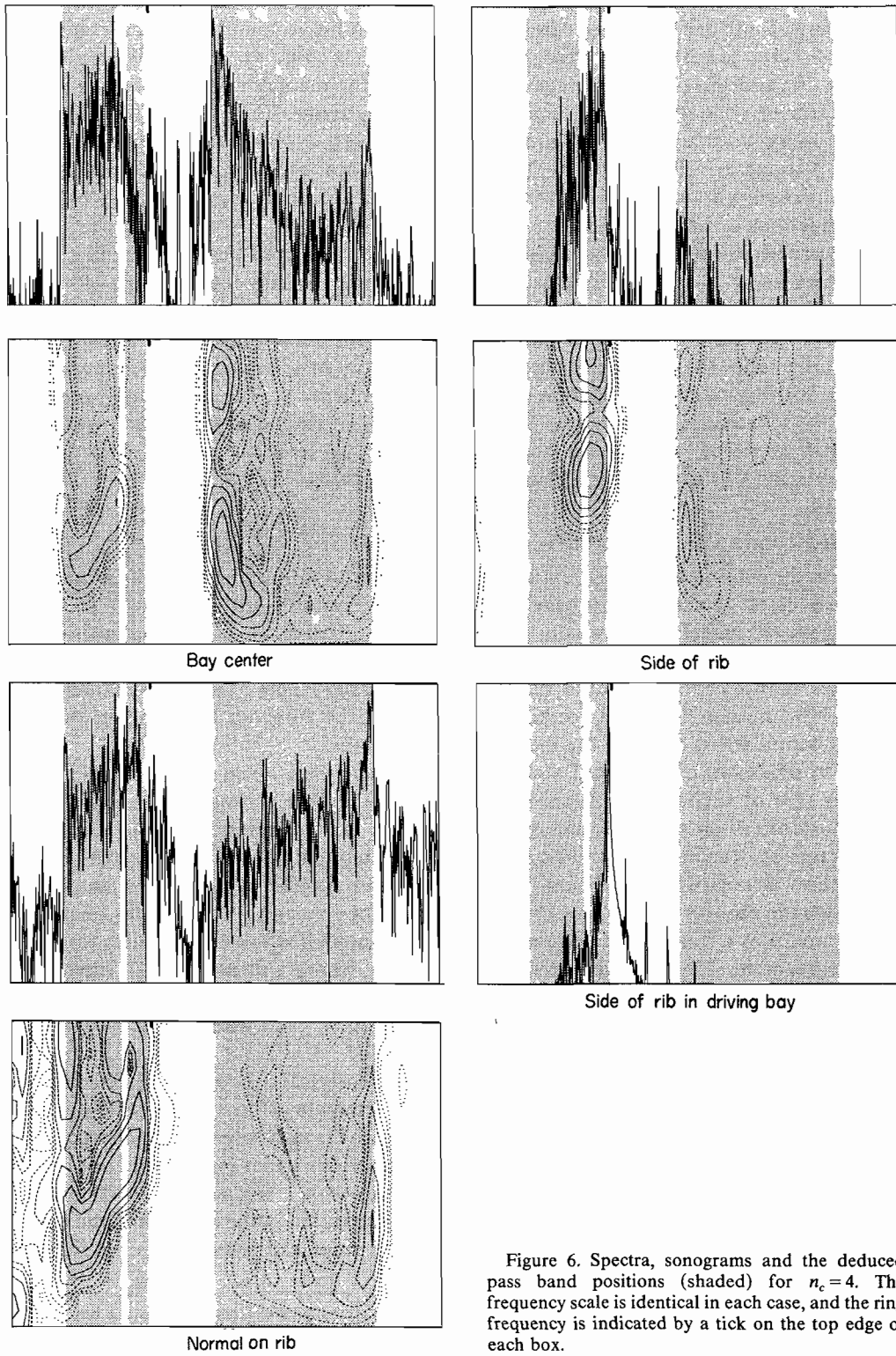


Figure 6. Spectra, sonograms and the deduced pass band positions (shaded) for $n_c = 4$. The frequency scale is identical in each case, and the ring frequency is indicated by a tick on the top edge of each box.

As an example of the data from which these band edge positions were deduced, Figure 6 shows a set of spectra and sonograms for $n_c = 4$. This figure contains seven pictures—the spectrum and corresponding sonogram for each of the three driving positions observed in bay 20, and the driving-bay spectrum in bay 6 for the side of the rib. Each picture (spectrum or sonogram) covers the same frequency range. The pictures are aligned in each column so that identical frequencies are in a vertical line. Superimposed on each set of pictures are shaded stripes showing the deduced positions of pass bands. It was found necessary to use the data from bay 37 as well as from bay 20 to be sure of all the identifications of band edges.

The process of deducing the edges shown in Figure 5 from all the data of which Figure 6 is an example is quite complicated, because one has to allow for the effect of “breakthrough” between different angular orders mentioned above. Once the complete picture has been built up, it is possible to label most of the features in the spectra such as those of Figure 6, either as genuine edges for that value of n_c or as breakthrough from a strong feature corresponding to a different (usually close) value of n_c . The sonograms are a great aid in the identification of the true bands for each n_c : it can be seen that they are a good deal less cluttered with noise, most of which is due to breakthrough. The detailed interpretation of these sonograms will be discussed below.

4.2. MEASURED AND THEORETICAL SONOGRAMS

While the band edge diagram is a very useful way of conveying a lot of information in one picture, it does not provide the clearest or the most stringent check of theory against measurements. The reason, as just described, is that to deduce the positions of these band edges from measured spectra requires quite a lot of interpretive effort. Thus while the authors believe that the diagram shown above (Figure 5) is a correct interpretation of the measurements, a sceptical reader could be forgiven for thinking that the interpretation was guided by the theoretical predictions.

The comparison of measured and theoretical sonograms, given in this subsection, is entirely free of such doubts. From the angular filtered time series, the calculation of a sonogram offers no scope for interpretation by the experimenter. Also, the theoretical sonograms are far more sensitive to details in the modelling than are the band edges. They show details within the pass bands rather than simply the position of the edges, and since the group velocity comes from the slope of the dispersion curves, the behaviour of the modes as a function of frequency needs to be modelled rather accurately to obtain good agreement. Thus the very detailed agreement which will be revealed makes the theoretical model quite convincing. To be shown, for selected values of n_c , are three sonograms corresponding to the three driving positions, each with the theoretical first arrival time as a function of frequency superimposed.

Figures 7(a)–(e) show the sets of sonograms and theoretical overlays for selected values of n_c . These values have been chosen in order to illustrate a few important features in the comparison between theory and experiment and are the same ones for which frequency versus axial wavenumber plots were shown in the previous paper (space does not permit the presentation of three sonograms for all 17 values of n_c). In each picture, the upper sonogram shows transmission from bay 8 to bay 20 measured in the bay centre, the centre sonogram shows transmission from bay 6 to bay 20 measured normally on the rib, and

Figure 7. Measured and theoretical sonograms, for the three driving positions used: top is the bay centre, middle is normal on the rib, and lowest is the side of the rib. The ring frequency is shown in each case by a tick on the top edge of the box. The meaning of the plotted symbols is explained in the text. (a) $n_c = 0$; (b) $n_c = 1$; (c) $n_c = 4$; (d) $n_c = 8$; (e) $n_c = 14$.



(b)

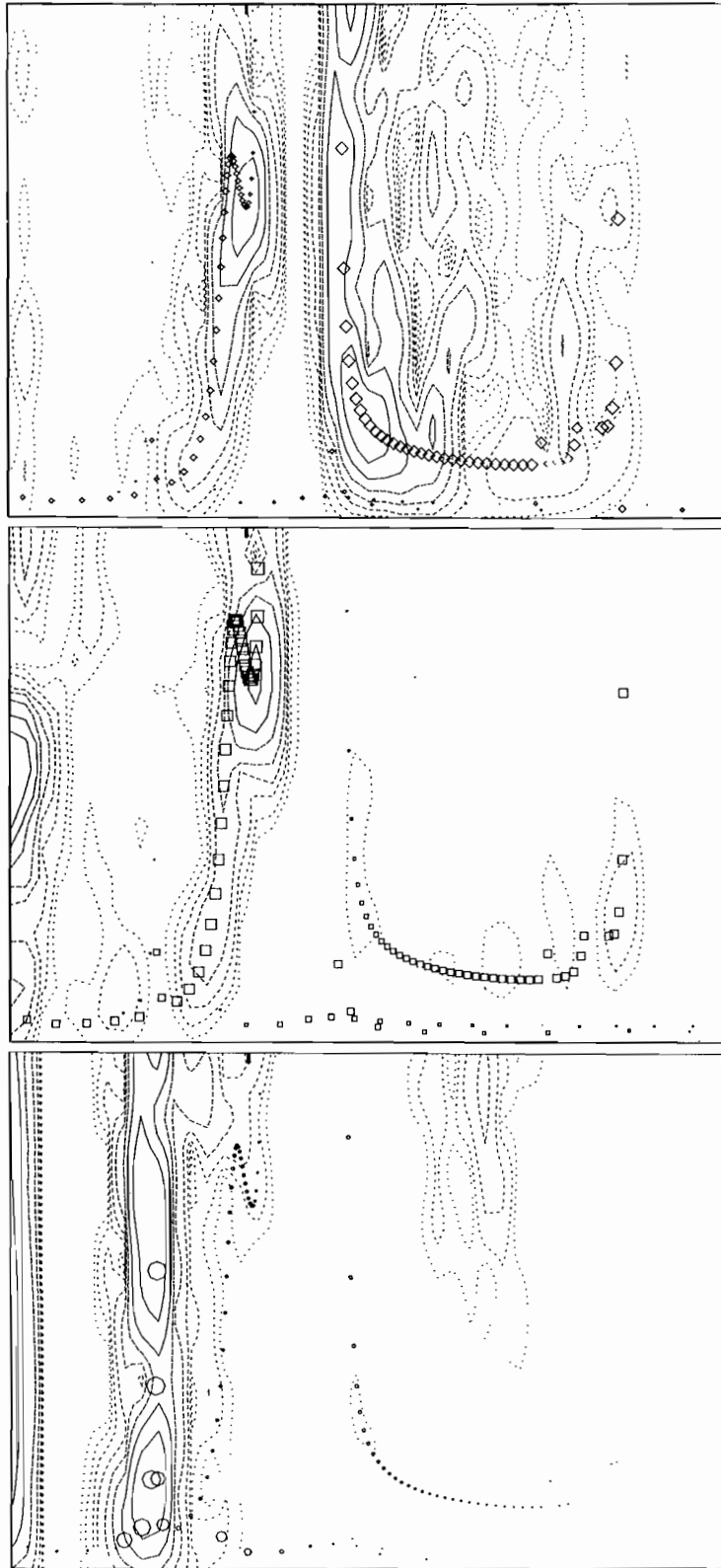


Figure 7 - continued.

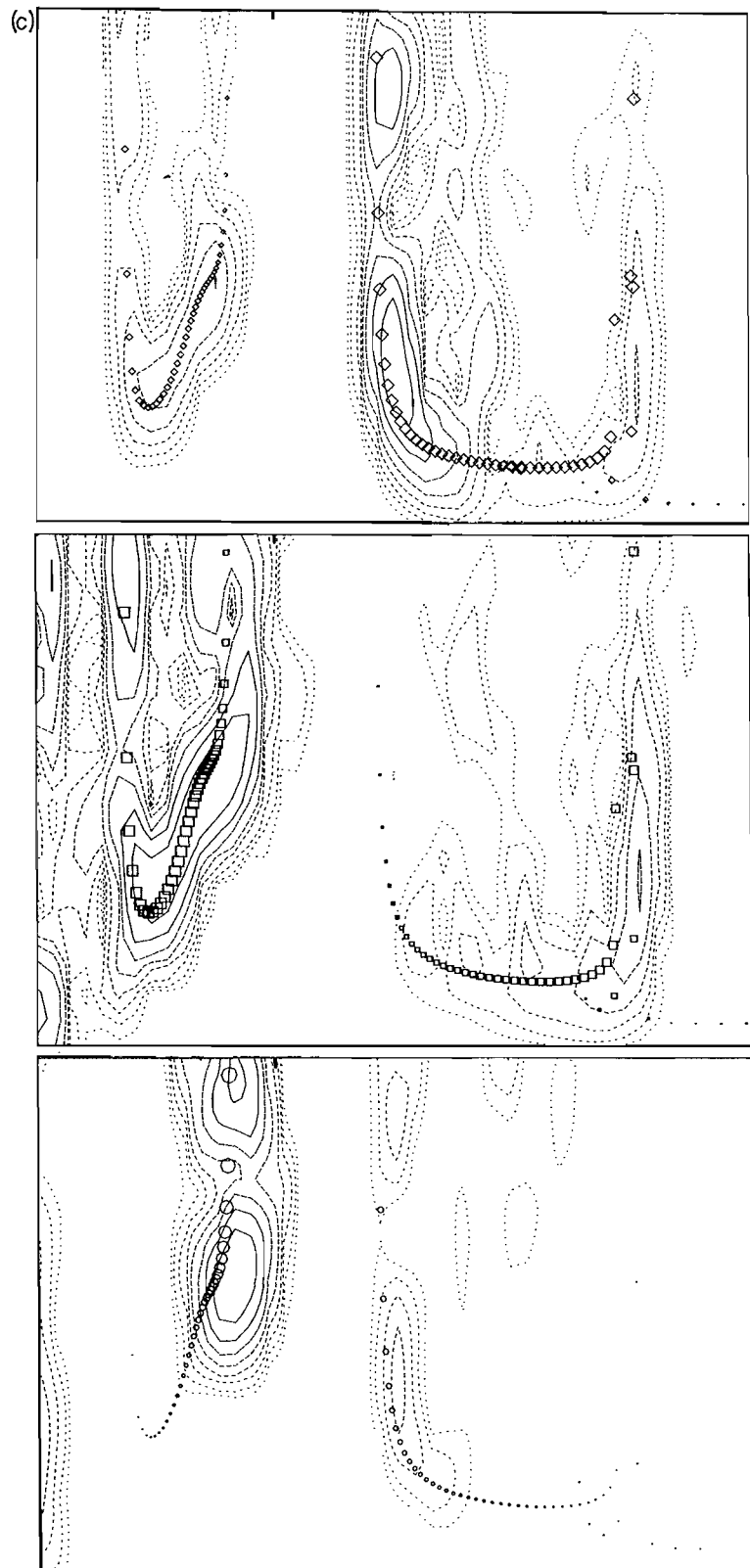


Figure 7 - continued.

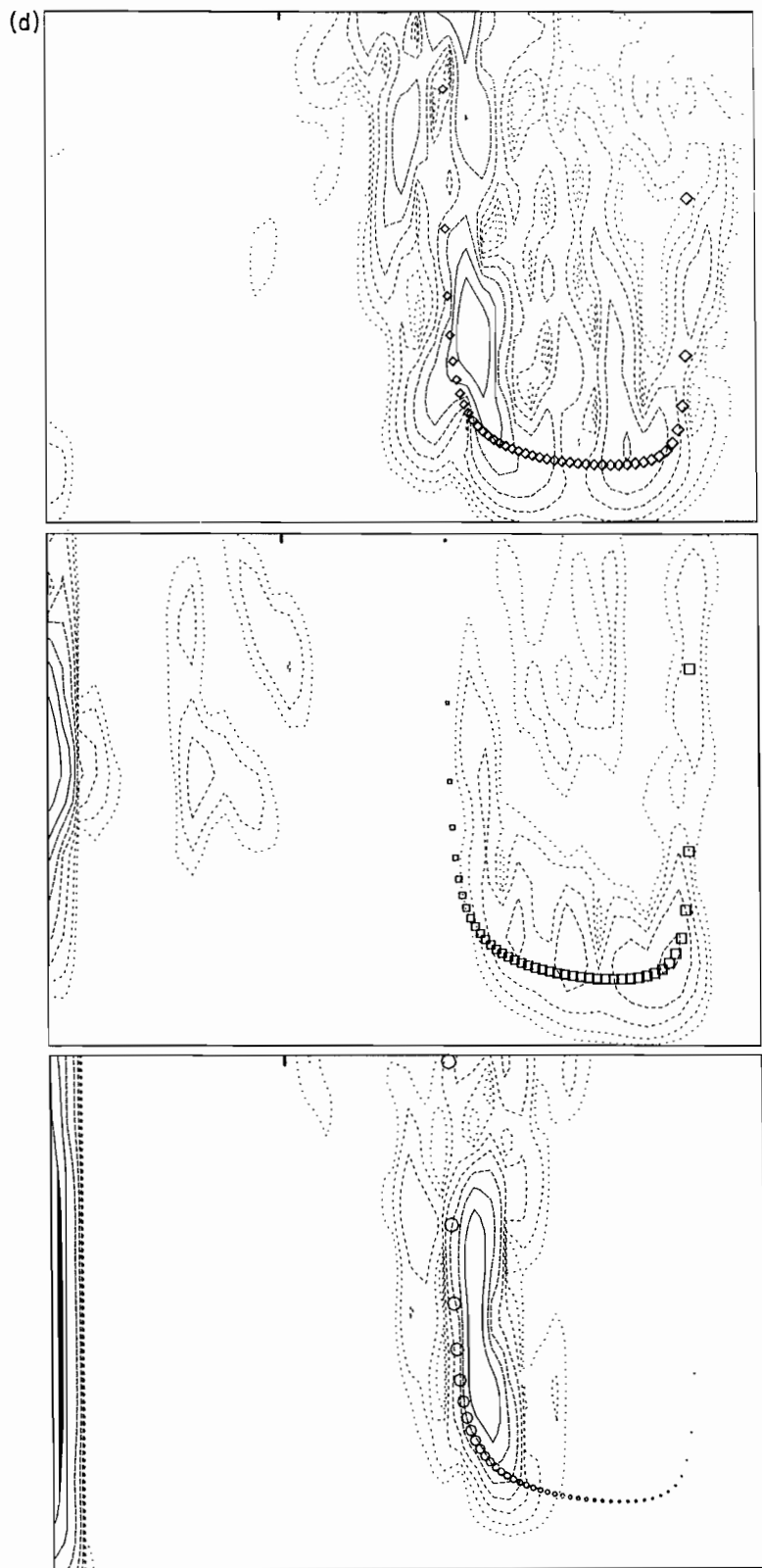


Figure 7 - continued.

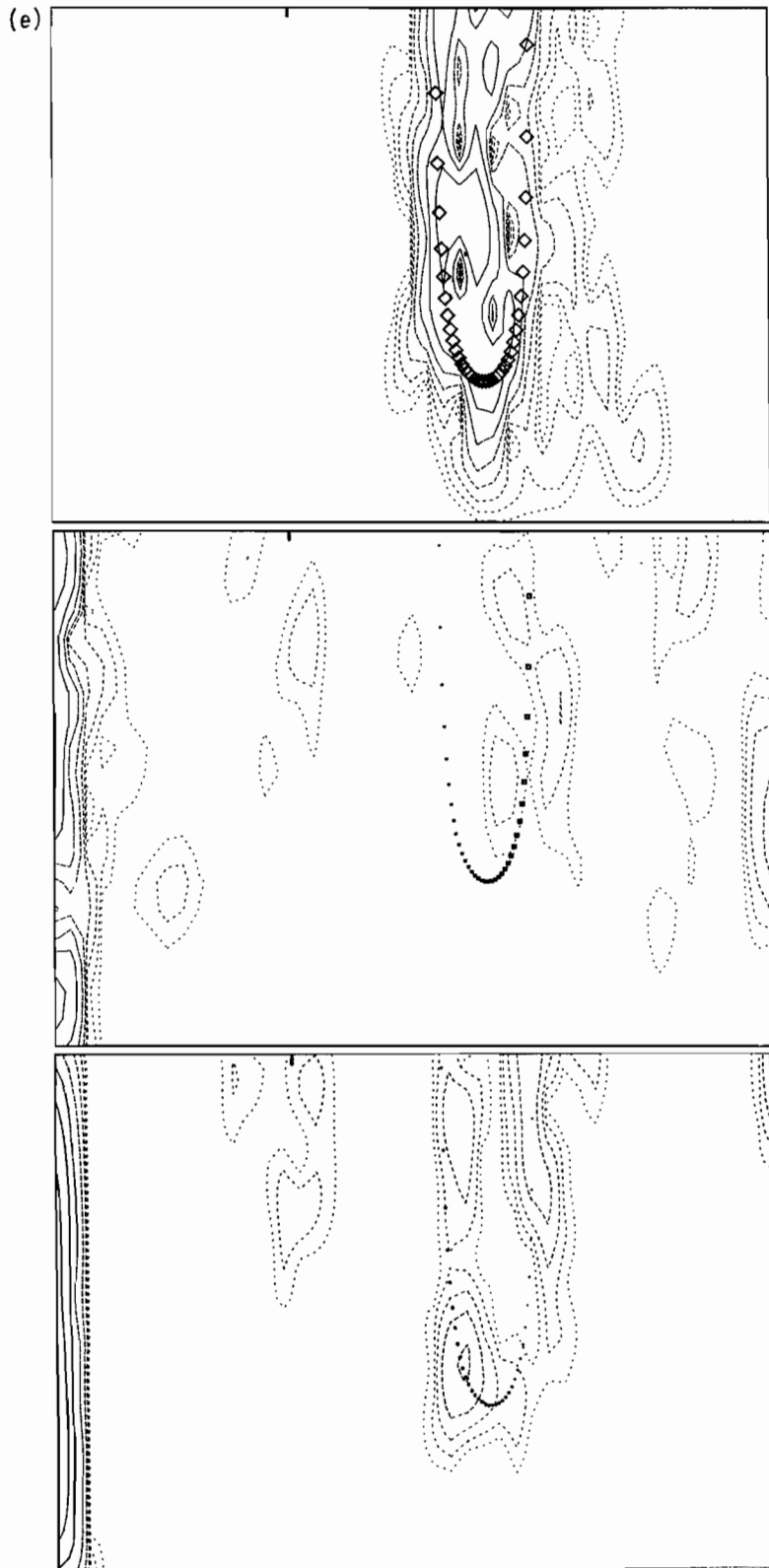


Figure 7 - continued.

the lower sonogram shows transmission from bay 6 to bay 20 measured on the side of the rib. Each picture has a time range of 0.0304 s starting from the moment of impact of the hammer. The measurements are in the form of contour plots, with eight contours spaced logarithmically at 3 dB intervals downwards from the maximum value in each individual picture. To aid the eye in interpreting which features are hills and which valleys in the contour maps, the highest contour in each case is solid, and the lower ones are in progressively shorter dashes.

The theoretical overlays take the form of discrete points, and three different plotting symbols are used for the three excitation positions (cf. the band edge pictures in reference [1]). The position of the symbol denotes the first arrival time at the observing point of the associated disturbance—later reflections from the ends of the finite cylinder are not shown. The spacing of the points is governed by axial wavenumber: a point is calculated corresponding to each mode of the actual structure (length 44 bays). Details of how the group velocities were calculated to give these sonograms are given in reference [1].

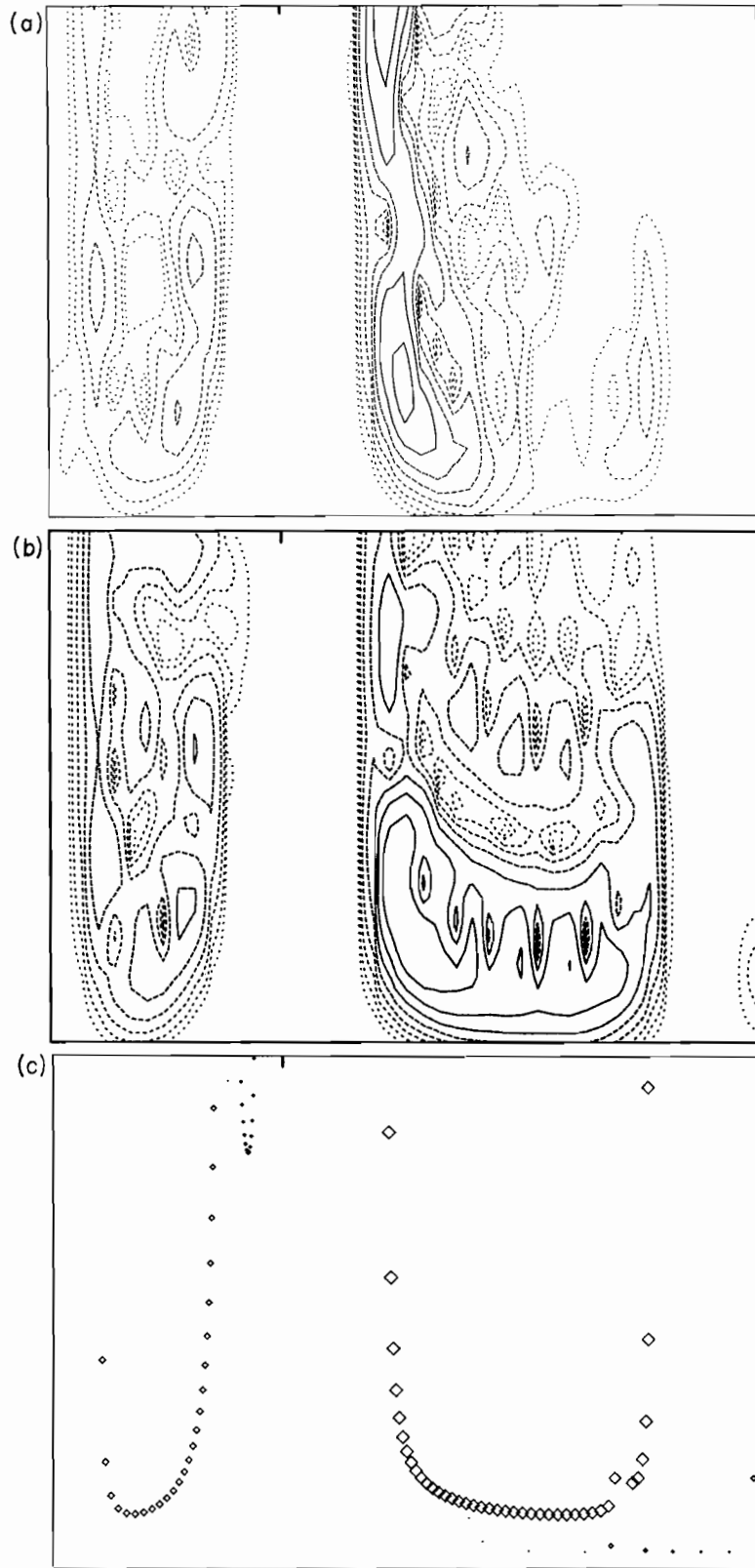
The sizes of the plotting symbols have been varied to give an indication of the mode shapes: in each case, the linear dimensions of the plotting symbol are proportional to the amplitude of motion to be expected in the excitation position being studied. For that reason, although the theoretical sonograms in each set of three show the same set of points with the same arrival times, they have quite different patterns of symbol sizes. The aim is that strong signals in each measured sonogram should correspond to a region of large plotting symbols in the associated theory.

When comparing the measurements with the theory, one must of course keep in mind that the measured sonograms cannot be as sharply defined as the theoretical lines—the Uncertainty Principle tells one that. The effect of windowing both in time and frequency is to smear out the lines of first arrival times into relatively broad bands. As described elsewhere [2], one can control the trade-off between time resolution and frequency resolution by choice of parameters in the sonogram calculation.

These remarks about windowing can be illustrated before proceeding to the detailed examination of different n_c values. Figure 8 shows (a) a typical measured sonogram (in fact for $n_c = 3$, measured at the bay centre, bay 8 to bay 20), (b) a similar contour map of a sonogram calculated from the theory, and (c) the usual theoretical overlay for this sonogram, showing the first arrival time as a function of frequency and with scaled plotting symbols to show modal amplitude. Thus (b) and (c) are different presentations of the same theory, except that (b) has all the windowing and multiple reflections taken into account in the same way as does the measurement, (a). In the theoretical model there is no attempt to include a realistic description of the ends of the cylinder [1] and it was necessary to make some rather *ad hoc* assumptions about boundary conditions there in order to produce (b). Obviously (b) gives in general the better comparison with the measured sonograms, but (c) is far better for showing superimposed on the measured sonograms since it is very hard to see what is happening in a pair of superimposed contour maps.

The main purpose of showing this three-way comparison of sonograms is simply to demonstrate that the pictures like (c) which will be used from now on do represent a good fit to the measured sonograms. While one is looking at this figure, however, it is also interesting to observe some detailed points of similarity and difference between (a) and (b). The main visible difference arises at the higher frequencies, simply from a roll-off in the force input by the soft hammer used in the measurements. Thus the general lowering of levels towards the right-hand side of (a) is of no physical significance.

Figure 8. Comparison of a measured sonogram (a) with two different presentations of the corresponding theoretical sonogram (b) and (c) (see text). The ring frequency is indicated by a tick in each case.



There are some very striking similarities between the two pictures, however, over and above the general shape also revealed by (c). The approximate distribution of peaks and dips in the response along the first arrival lines is well reproduced—in fact as well as could be hoped in view of the rather *ad hoc* assumptions about boundary conditions at the ends of the cylinder which had to be made to produce (b). Also, with the comparison (b) at hand, one can see quite clearly in (a) traces of the first-reflected signals from the two ends of the cylinder in the form to be expected from the discussion in reference [2].

One can now look at the comparisons of theoretical and measured sonograms for the selected values of n_c in Figures 7(a)–(e). One can start with $n_c = 0$, although this is actually a somewhat atypical case. The first remark is that the three measured sonograms look quite different, but that in each case the theoretical overlays agree quite well with the areas of strong signal. To understand the features one can refer to Figures 3 and 5. In the bay centre sonogram, one sees most clearly the band running from line (c) to line (i) in the former figure. It is clear from the sketches corresponding to those lines (Figure 2) that both have considerable bay centre motion. Also visible is some activity around the ring frequency, which one might expect to see when $n_c = 0$. Notice that little is visible below the ring frequency in either of the top two sonograms, although according to the theoretical plots there is a pass band extending down to zero frequency, and for higher values of n_c the first band *will* show up in these sonograms down to its cut-off frequency. The reason for this is that the character of the motion changes at these low frequencies to be dominated by in-surface motion. It should be noted that most of the sonograms show some signal near zero frequency—this is generally an artefact of the integration performed to obtain velocity (power) spectra from acceleration measurements.

The normal rib motion sonogram also shows this ring frequency activity, but shows no trace of the lower edge of the band around line (c) which was so strong in the bay centre. The reason for this is clear from the motion sketches: (c) has indeed no normal motion of the rib. Thus the third band “fades out” towards its lower edge in this sonogram (the top edge being clearly visible). It should be noted that all the rib normal sonograms come from hard hammer data rather than soft hammer data, which means they extend to rather higher frequencies, but on the other hand the data was less good because of a clipping problem so that the sonograms are less clear. The sonogram for the side of the rib is quite different again: this time the only really strong motion is in the vicinity of the rib resonance, as one might expect. Thus there are very large symbols at the frequencies labelled “rib resonance” in the theoretical plot.

The same kind of discussion can be given for the other values of n_c shown. Comparisons of the sets of sonograms with the theoretical plots will in each case show what the character of the motion is at different frequencies, and will thus explain which features are strong in the various measurement positions. Further comment is restricted only to a few general features of the data. The first of these is the rather curious shape of the first band sonogram for $n_c = 4$ which is rather well modelled by the theory. This feature is of little significance, no doubt, but it is an example of the small details of behaviour, brought out by the sonogram analysis technique, which are very sensitive to details in the theoretical model and therefore provide the most stringent check on the theory. Incidentally, notice that these sonograms for $n_c = 4$ are the same as the ones appearing in Figure 6 above.

The next general point relates to the rib resonance band—for most values of n_c it is not visible in the sonograms. The reason is simply that it is usually a very narrow band, and narrow bands have correspondingly low group velocities (group velocity being proportional to the inverse of modal density). Thus the first arrival time corresponding to the rib resonance band is usually outside the time window. To see the rib resonance band one must use the spectra, as illustrated in the previous subsection. The point about

narrow bands having slow group velocities is well made by the behaviour of the first band as n_c passes through the value 8: the band goes through a minimum width at that value, and indeed the sonograms for $n_c = 8$ do not show the first band which has gone off the top of the plot. This value of n_c also shows the worst *disagreement* between theory and measurements for any of the sonograms (including those not shown here): the lower edge of the third pass band is not quite correctly placed. The extent of this disagreement is not serious. Investigations of the sensitivity of the theoretical predictions to the physical dimensions show that errors of the magnitude revealed here are broadly consistent with known accuracy of dimensions in fabrication of the ribbed cylinder, and with other approximations made in the modelling process.

The final general point to which attention is drawn relates to the character of the first band at higher values of n_c . One can see very clearly the change to a clamped bay mode which has occurred by $n_c = 14$. The bay centre sonogram reveals uniformly strong motion throughout a rather symmetrically shaped first band which is now the only one lying in the frequency range. Both of the other sonograms show much smaller motion, corresponding to the near clamping of the ribs. Also, it is clearly visible from the theoretical overlays that the lower edge of the band corresponds to rib twisting (side of the rib showing stronger motion) while the upper edge corresponds to rib bending (normal rib motion stronger). All of this is in accordance with the qualitative discussion of section 2.

5. CONCLUSIONS

In this paper measurements of vibrations of a ribbed cylinder have been described and compared with the parallel theoretical modelling of reference [1]. Very good detailed agreement has been exhibited for the behaviour of the various angular orders for propagation along the cylinder over the frequency range from zero up to about three times the ring frequency. This agreement has been displayed both in the behaviour of the edges of the pass bands as a function of circumferential wavenumber and in the group velocities as a function of frequency for each separate angular order.

In order to obtain this level of agreement between theory and measurement, it was found necessary to model the geometry of the T-section ribs in some detail. The main reason for this is that the first cross-sectional resonance of the ribs, a cantilever bending mode, falls well within the frequency range studied. To allow for this, suitable additional degrees of freedom were needed in the (variational) model used in the theoretical work. To extend the work to higher frequencies, further such degrees of freedom would have to be allowed for as more and more internal resonances of the ribs need to be included.

ACKNOWLEDGMENTS

This work has been carried out with the support of the Procurement Executive, Ministry of Defence. The authors are particularly grateful to Dr I. Roebuck for helpful discussions and much patience during this programme of work. We also thank Professors D. G. Crighton and J. E. Ffowcs Williams for useful comments.

REFERENCES

1. C. H. HODGES, J. POWER and J. WOODHOUSE 1985 *Journal of Sound and Vibration* **101**, 219-235. The low frequency vibration of a ribbed cylinder, Part 1: Theory.
2. C. H. HODGES, J. POWER and J. WOODHOUSE 1985 *Journal of Sound and Vibration* **101**, 203-218. The use of the sonogram in structural acoustics, and an application to the vibrations of cylindrical shells.

3. R. N. ARNOLD and G. B. WARBURTON 1949 *Proceedings of the Royal Society* **A197**, 238-256. Flexural vibration of the walls of thin cylindrical shells having freely supported ends. (Reprinted in A. KALNINS and C. L. DYM 1976 *Benchmark Papers in Acoustics*, Volume 8, Stroudsburg, Penn: Dowden, Hutchinson and Ross.)
4. LORD RAYLEIGH 1877 *The Theory of Sound*, Volume 1. New York: Dover. Second edition 1945 re-issue. See article 192.
5. L. BRILLOUIN 1946 *Wave Propagation in Periodic Structures*. New York: McGraw-Hill.
6. D. J. MEAD 1975 *Journal of Sound and Vibration* **40**, 19-39. Wave propagation and natural modes in periodic systems: II, Multi-coupled systems with and without damping.
7. C. H. HODGES and J. WOODHOUSE 1983 *Journal of the Acoustical Society of America* **74**, 894-905. Vibration isolation from irregularity in a nearly-periodic structure: theory and measurements.